AGU PUBLICATIONS

JGR

Journal of Geophysical Research: Atmospheres

RESEARCH ARTICLE

10.1002/2014JD022916

Key Points:
- A seeder-feeder and freezing drizzle episodes was registered
- This episode has been analyzed with the WRF model
- Cloud top temperature is strongly connected with precipitation type

Correspondence to:
S. Fernández-González,
sefern04@ucm.es

Citation:
Fernández-González, S., F. Valero, J. L. Sánchez, E. Gascón, L. López, E. García-Ortega, and A. Merino (2015), Analysis of a seeder-feeder and freezing drizzle event, *J. Geophys. Res. Atmos.*, *120*, 3984–3999, doi:10.1002/2014JD022916.

Received 1 DEC 2014
Accepted 7 APR 2015
Accepted article online 10 APR 2015
Published online 12 MAY 2015

Analysis of a seeder-feeder and freezing drizzle event

S. Fernández-González[1], F. Valero[1], J. L. Sánchez[2], E. Gascón[2], L. López[2], E. García-Ortega[2], and A. Merino[2]

[1]Department of Astrophysics and Atmospheric Sciences, Faculty of Physical Sciences, Complutense University of Madrid, Madrid, Spain, [2]Atmospheric Physics Group, IMA, University of León, León, Spain

Abstract Surface icing can cause dramatic consequences on human activities. What is more, numerical weather prediction models are not very accurate in determining freezing drizzle, which creates uncertainty when forecasting this type of weather phenomenon. Therefore, it is essential to improve the forecast accuracy of these models for such phenomena to mitigate risks caused by unforeseen freezing drizzle events. On 5 February 2012, an episode of freezing drizzle took place in the Guadarrama Mountains, at the center of the Iberian Peninsula. This episode was preceded by weak snowfall. After the freezing drizzle, moderate snowfall was recorded in the study area. This event was simulated using the Weather Research and Forecasting model. Through this analysis, we identified the meteorological factors at both synoptic scale and mesoscale that caused this episode. Wind perpendicular to an orographic barrier-generated updrafts and retention of moisture upwind, which caused orographic clouds to appear on the north side of the Guadarrama Mountains. Atmospheric stability prevented cloud formation at midlevels at the time of the freezing drizzle, which maintained cloud top temperatures warmer than −15°C during the episode. The entrance of moisture and instability at midlevels caused cloud top temperatures substantially colder than −15°C, which coincided with snow in the mountain range. Cloud top temperature and thickness control the efficiency of the glaciation process, thereby determining the type of precipitation at the surface. Freezing drizzle risk and in-cloud icing algorithms were developed with the aim of predicting similar events in the study area, which could mitigate impacts on human activities.

1. Introduction

Freezing precipitation and in-cloud icing can cause ice accretion, with consequent adverse effects on transport (freezing drizzle causes a very high risk of road accidents [*Norrman et al.*, 2000]), and may cause deaths and economic loss [*Zhou et al.*, 2013].

The main synoptic-scale regions associated with the formation of freezing drizzle are in the overrunning region of a warm front, near a low-pressure center, and at the leading edge and toward the rear of cold fronts [*Bernstein et al.*, 1998]. Freezing drizzle is common at high latitudes, because conditions are favorable for its development more frequently. In the northern United States and Canada, freezing rain is common [*Roebber and Gyakum*, 2003; *Henson et al.*, 2007], although it can also occur at midlatitudes [*Sun and Zhao*, 2010]. Because of its milder climate, freezing precipitation events in southwestern Europe are virtually restricted to high altitudes [*Carrière et al.*, 2000], as in the case analyzed here.

During the TEcoAgua project, a freezing drizzle and seeder-feeder event was recorded on 5 February 2012, between 11:00 and 13:30 UTC. This event was between two periods of snow recorded at the surface. Observation of this episode using TEcoAgua instrumentation has been described in detail in *Fernández-González et al.* [2014b]. This observation demonstrated that surface icing was originated by the warm rain process; therefore, in this paper we will only consider surface icing caused by this process.

The warm rain process, whereby droplets of liquid water develop through collision-coalescence processes, is characteristic of clouds composed almost entirely of liquid water with cloud top temperatures warmer than −15°C [*Cortinas et al.*, 2004]. These conditions favor the formation of supercooled drops, owing to the low concentration of active ice nuclei at such temperatures, which makes the warm rain process responsible for most episodes of freezing drizzle [*Bernstein*, 2000; *Rauber et al.*, 2000].

Freezing drizzle occurs when supercooled drops of diameter approximately 40–400 μm reach the surface, where temperatures are subfreezing [*Marwitz et al.*, 1997]. Supercooled drops are thermodynamically

unstable with respect to the solid phase [*Lamraoui et al.*, 2013], so if they contact a solid surface, an ice crystal, or freezing nuclei, they will change to solid phase [*Rock*, 2003].

Conditions necessary for freezing drizzle formation are warm cloud tops (−15°C or warmer), stable stratification, weak mesoscale uplift, and ice crystal concentrations $< 1\ L^{-1}$ [*Cober et al.*, 1996]. Orographic barriers generate upslope flow [*Stuart and Isaac*, 1999] and favor freezing drizzle at the local scale, generally upwind of mountains [*Mott et al.*, 2014]. Ice or snow on the surface helps maintain freezing conditions there, facilitating formation of a thermal inversion layer in the first few meters above the ground, increasing the likelihood of freezing drizzle [*Strapp et al.*, 1996].

As occurred in the Guadarrama Mountains, high-altitude mountain ranges may be located above cloud base, which may cause in-cloud icing if the surface temperature is less than 0°C [*Niu et al.*, 2012]. Not surprisingly, in-cloud icing occurs most often in mountainous areas and coastal zones at high latitude [*Yang et al.*, 2012]. The main problems caused by such icing are ice accumulation on rotor blades of wind turbines [*Laakso et al.*, 2010] and on electrical wires [*Thorkildson et al.*, 2009].

The presence of ice crystals can deplete cloud droplets via riming and deposition, thereby inhibiting drizzle formation [*Geresdi et al.*, 2005] and reducing the risk of surface icing. In fact, experimental measurements have demonstrated enhanced scavenging of liquid water within orographic clouds by ice crystals from aloft [*Roe*, 2005]. These ice crystals can be provided by the "seeder-feeder" mechanism, which was defined by *Reinking and Boatman* [1986] as the phenomenon by which the lower cloud is microphysically stimulated by and feeds moisture to the natural ice "seeds" supplied by the upper cloud. The introduction of ice nuclei from the upper cloud initiates precipitation in the low-level liquid cloud layer, so precipitation is augmented over the mountain [*Robichaud and Austin*, 1988]. In the feeder cloud, precipitation is enhanced primarily by depositional growth via the Bergeron-Findeisen process, collision-coalescence in warm rain processes or aggregation in cold cloud processes, and by accretion/riming [*Castellano et al.*, 2004].

The principal meteorological variables needed to estimate ice accretion are rain rate, surface temperature, and wind velocity, which can be estimated by numerical weather prediction models [*Hosek et al.*, 2011]. Forecasting freezing precipitation is challenging because of the small scale at which its causative processes develop, compared with the grid resolution of common numerical weather forecasting models [*Carrière et al.*, 1997]. Owing to the growing capacities of atmospheric models, great efforts have been made in recent years to collect icing field data for calibration, statistical analysis, and modeling [*Makkonen*, 2000; *Makkonen and Lozowski*, 2008]. A low spatial resolution may underestimate the orographic forcing [*Fargey et al.*, 2014], so the use of weather forecasting models with high spatial resolution can improve the forecasting of variables key to the development of these phenomena, such as liquid water content (LWC) within clouds [*Fikke et al.*, 2008; *Thompson et al.*, 2008].

The Weather Research and Forecasting (WRF) model has been used to analyze freezing precipitation events [*Hosek et al.*, 2011; *Podolskiy et al.*, 2012]. The WRF model permits selection of several microphysics options to determine the precipitation type expected at the surface, although variables useful for determining freezing precipitation are not usually included in the standard output parameters of WRF. Therefore, use of precipitation-type algorithms is required to define the type of hydrometeor expected at the surface [*Musilek et al., 2009*]. Because of serious personal and economic damage that can result from freezing precipitation events [*Yang et al.*, 2008], it is important to forecast such events using numerical models to mitigate the damage.

In the present paper, we analyzed the interaction between synoptic-scale and mesoscale conditions as well as microphysical processes using WRF to study factors leading to the freezing drizzle episode. Having identified these factors, we developed a simple algorithm to analyze future such episodes.

2. Meteorological Modelization

The TEcoAgua field project was implemented during winter 2011/2012 in the Guadarrama Mountains, which are at the center of the Iberian Peninsula (Figure 1). This mountain range has a southwest-northeast orientation, with maximum altitudes over 2000 m above sea level (asl) An icing event was recorded at altitude 1880 m asl, only 800 m northwest of Navacerrada Pass, which connects the provinces of Madrid and Segovia as well as the Lozoya Valley. Because of its close proximity to a major urban center (Madrid is 50 km away), this area has a large influx of tourists, especially in winter since it gives access to two ski areas. These factors increase the region's vulnerability to risks such as heavy snow or freezing precipitation.

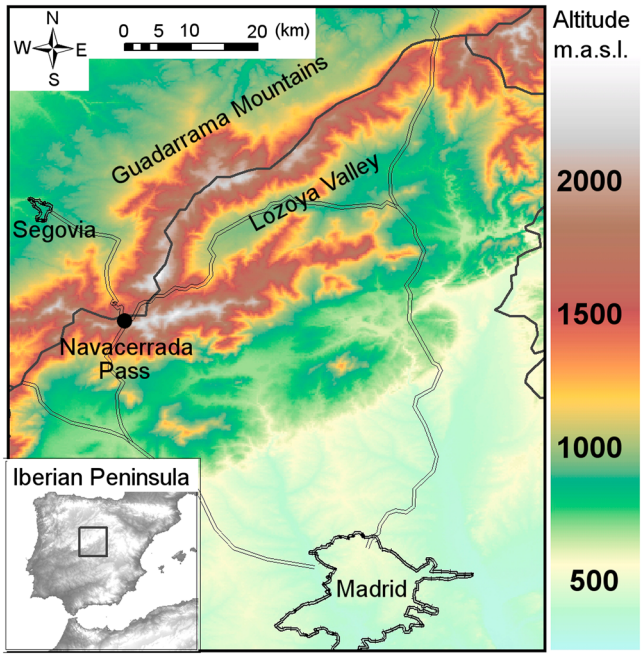

Figure 1. Map of study area, with its location on the Iberian Peninsula shown in the bottom left panel.

Meteorological conditions affecting the Guadarrama Mountains on 5 February 2012 were simulated with version 3.1.1 of the Advanced WRF, a nonhydrostatic, three-dimensional model [*Skamarock et al.*, 2008]. Details of the numerical schemes in this model can be found in *Skamarock and Klemp* [2008]. Mesoscale models are commonly used in the forecasting and evaluation of seeder-feeder and freezing drizzle episodes [*Thompson et al.*, 2004].

Initial and boundary conditions were provided by the National Centers for Environmental Prediction Global Forecast System (with 1° horizontal grid spacing, updated every 6 h). This analysis used data from the surface and 26 pressure levels between 1000 and 10 hPa. This global reanalysis data set has been used in similar studies [*Podolskiy et al.*, 2012; *Viale et al.*, 2013].

The WRF model was initialized at 00:00 UTC on 5 February 2012 and was run for 24 h of physical time, giving the model a few hours to stabilize before the key period of the analyzed episode. A total of 82 sigma levels were defined to study meteorological conditions in the troposphere, including 16 levels in the lowest 1 km giving highest resolution near the ground, similar to the configuration of *Nygaard et al.* [2011] and *Yang et al.* [2012]. For shortwave radiation, the scheme described by *Dudhia* [1989] was used, whereas for longwave radiation we used the Rapid Radiative Transfer model [*Mlawer et al.*, 1997]. We also used the Noah Land Surface Model [*Chen and Dudhia*, 2001] and Eta surface layer scheme defined by *Janjic* [1996]. After comparing different microphysical parameterizations, we chose the Goddard scheme [*Tao et al.*, 2009] because it best explained the concentrations of liquid water and ice in the study area during winter. This model and similar parameterizations have been previously tested in the area, with satisfactory results [*Gascón et al.*, 2015].

Four nested domains were defined (Figure 2) to achieve high spatial resolution. *Nygaard et al.* [2011] showed that by increasing this resolution, estimation of LWC in clouds is significantly improved. The synoptic environment was described using domains D01 and D02. D01 covers southwestern Europe, with 100 east-west grids and 103 north-south. This domain had spatial resolution 27 km and the interval between outputs was 3 h. Domain D02 covered the entire Iberian Peninsula, with 133 east-west grids and 115 north-south. The spatial resolution of 9 km was useful for locating various air masses affecting the peninsula on the study day. D03 was

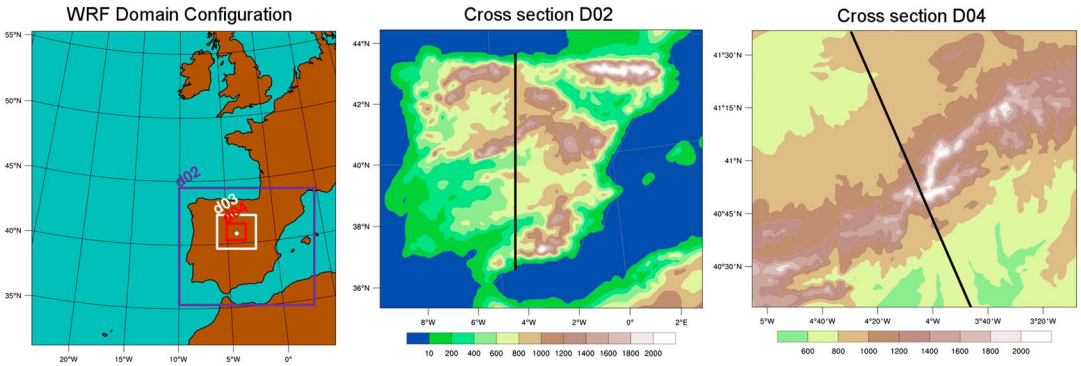

Figure 2. (left) Domains of WRF model and cross sections in (middle) D02 and (right) D04. White point in Figure 2 (left) shows location of Navacerrada Pass.

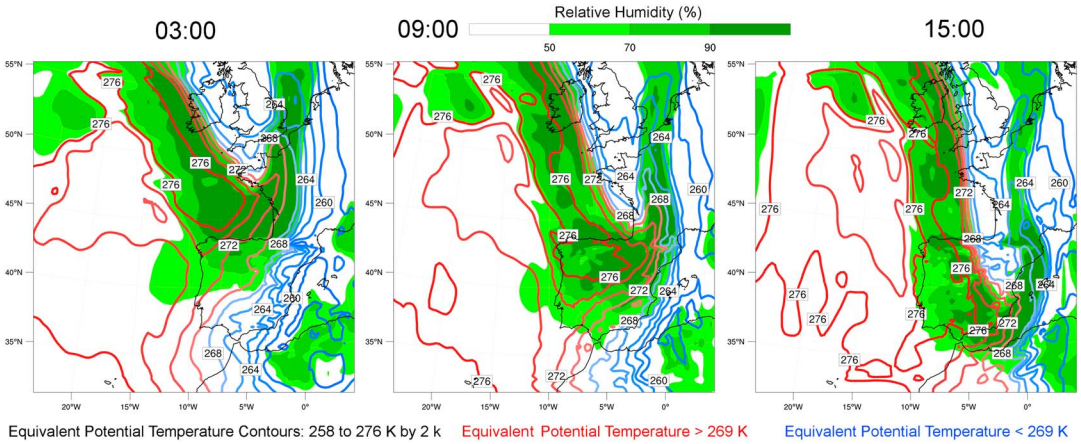

Figure 3. The θ_e (contours, in K) and RH (shaded, in percent) modeled in D01 domain of WRF. The θ_e contours are colored to differentiate warm and cold air masses.

defined as intermediate between the synoptic-scale and the high-resolution D04. D03 had spatial resolution 3 km, with 115 east-west grids and 100 north-south. Although D03 was not used to describe the episode, it was necessary to define it for maintaining proportionality between domains and attaining the high resolution of D04. The latter domain was optimal for precisely analyzing mesoscale factors that induced the fall of freezing drizzle and the seeder-feeder process. This domain had spatial resolution 1 km and was composed of 169 east-west grids and 148 north-south. The interval between outputs of domains D02, D03, and D04 was 1 h.

To analyze the arrival on the Iberian Peninsula of air masses with different thermodynamic properties, we constructed a north south cross section across D02. This orientation was chosen because it approximates the trajectory of warm air advection that caused the icing. The cross section traversed Navacerrada Pass (where precipitation in the form of freezing drizzle was observed), roughly following the 4°W meridian. This vertical section spanned 43.5°N through 36.5°N. To analyze meteorological conditions near the study area, we made a cross section across D04 perpendicular to the Guadarrama Mountains, via Navacerrada. This cross section traversed 41°30′N, 4°40′W through 40°20′N, 3°40′W. It was decided to make a cross section perpendicular to the Guadarrama Mountains because this was the prevailing wind direction at the surface during the freezing drizzle episode.

3. Synoptic Overview

Using domains D01 and D02 modeled by the WRF, we analyzed the synoptic situation framing the freezing drizzle and seeder-feeder episode. Figure 3 shows relative humidity (RH) and equivalent potential temperature (θ_e) at the 700 hPa level in D01. This level is adequate for identifying the arrival of air masses with various thermodynamic properties [*Browning*, 1997], since the peaks of the Guadarrama Mountains are below it. The 700 hPa θ_e field has been used previously to identify different air masses [*Jenkner et al.*, 2010]. Using conservative variables enables identification of air masses and of different air parcels along their route, since the properties of temperature and moisture are combined. This is useful when distinguishing air masses with differing thermodynamic properties. θ_e is used as a conservative temperature for moist air, for which phase conversions are permitted [*Heimann*, 1992].

In the days before the icing event, a cold and dry air mass arrived on prevailing northeasterly winds, causing advection of a continental polar air mass. This air mass from Central Europe remained over the Iberian Peninsula (mostly over its eastern half) in the early hours of the study day, as seen in the image at 03:00 UTC (Figure 3).

In the image at 09:00 UTC, it is clear that the synoptic-scale situation in southwest Europe was dominated by a strong ridge centered over the Atlantic Ocean, which favored winds with a northerly component. This caused the arrival on the peninsula of an air mass from the Atlantic that was warmer and more humid than the continental polar air mass present during the previous days. By this time, the warm moist air mass had extended over the northern half of the peninsula. Earlier studies have linked onshore flow with freezing precipitation [*Stuart and Isaac*, 1999]. *Robbins and Cortinas* [2002] noted that air masses for which freezing

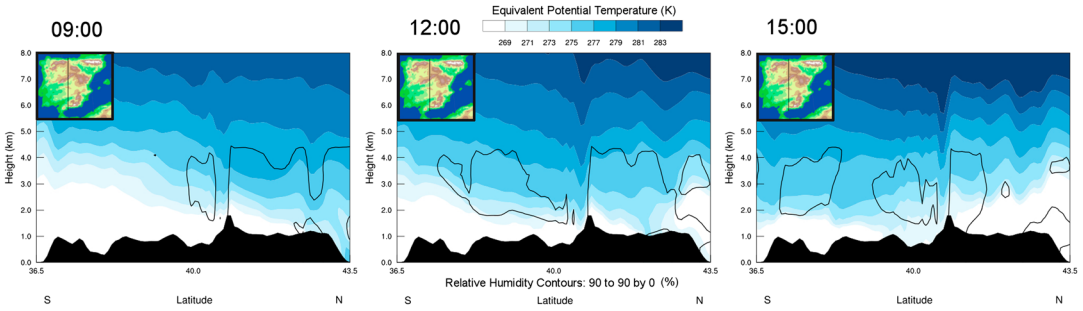

Figure 4. Cross section of D02 showing RH (contours, in percent) and θ_e (shaded, in K). Underlying Orography is solid black. Direction of cross section is shown in the top left.

precipitation is most frequent are continental polar in the case of cold air at the surface, and maritime polar for warm air aloft, which was the case with the air masses over the peninsula during the studied event.

Subsequently, lowering toward the south of an Arctic air mass led to the arrival of cold, dry air. The temperature contrast between the two air masses can be observed in the 15:00 UTC image (Figure 3), from the proximity of θ_e isotherms. *Bernstein et al.* [1998] indicated that the leading edge of a cold front is an area conducive to freezing precipitation.

The same conservative variables as in the case above are shown in Figure 4, but in this case were along the north-south cross section of D02. In the image at 09:00 UTC, the continental polar air mass persisted over the Iberian Peninsula. However, the slope of θ_e isotherms reveals the arrival from the north of a warmer air mass. The moisture transported by that warm air mass had already reached the Guadarrama Mountains (which are represented by the highest peak of this cross section), with RH near saturation evident to about 4 km.

The image at 12:00 UTC reveals the warm sector location over the peninsula, similar to the freezing precipitation episode with the warm sector ahead of a cold front described by *Roberts and Stewart* [2008]. However, cold air damming on the north side of the Guadarrama Mountains favored the persistence of temperatures colder than 0°C upwind of the mountain range, facilitating freezing precipitation. This is consistent with *Minder et al.* [2011] and *Erfani et al.* [2014].

Finally, in the image at 15:00 UTC, the pronounced inclination of θ_e over the northern half of the peninsula signaled the arrival of a cold and dry air mass, which had almost reached the Guadarrama Mountains at this time. Undulations of the θ_e isotherms downwind of the orographic barrier appear to indicate the presence of gravity waves. The low RH on the leeward side of the mountains was probably caused by the Foehn effect, which caused a warmer and drier environment there, consistent with *Hewson* [1998].

In summary, advection of a warm and moist air mass from the Atlantic Ocean led to increased instability upon being forced to rise above a cold, dry air layer over the Iberian Peninsula, which resulted from cold advection from Central Europe during the previous days. This also occurred in the cases of freezing precipitation analyzed by *Kajikawa et al.* [2000]. As with the "cold air damming with anticyclone" pattern for North America described by *Rauber et al.* [2001], warm air from the ocean ascended over cold air remaining inland, which was dammed along the north slope of the orographic barrier.

4. Mesoscale

To analyze mesoscale meteorological conditions on 5 February 2013, we used D04 because its high spatial resolution (1 km) facilitates analysis of meteorological phenomena developed or modified by small-scale processes. *Drage and Hauge* [2007] indicated that a grid of 1 km × 1 km is adequate to analyze cases of icing in mountainous areas.

4.1. Surface Pressure and Wind

Figure 5 shows surface pressure and wind at 10 m height. It is seen that at 09:00 and 12:00 UTC, the prevailing wind was westerly and weak, making it difficult for the air mass to cross the orographic barrier. Therefore, in the central and eastern Guadarrama Mountains, the wind veered to the southwest direction (parallel to the mountain range). This caused moisture advection at low levels and orographic enhancement, which favors the formation of orographic clouds upwind of the mountains.

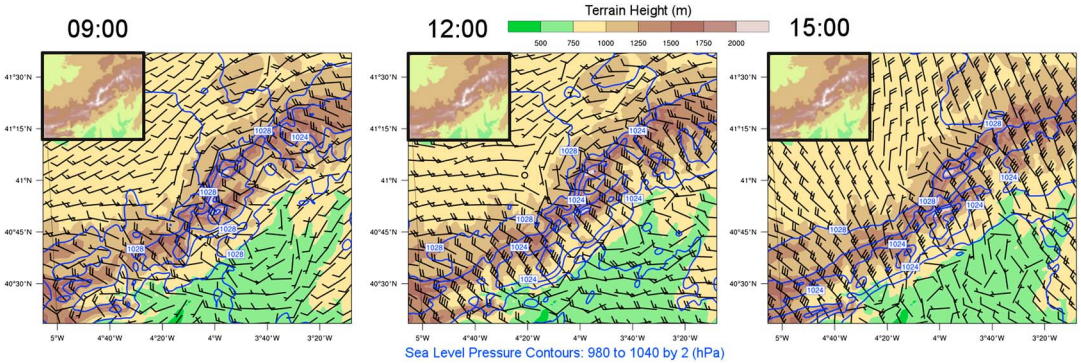

Figure 5. Surface pressure (hPa) and wind at 10 m above surface (m s^{-1}) in D04. Orography of D04 is underlain and shown in the top left.

The orographic barrier caused a block because of the weak airflow, as described by *Gross* [1994]. On several occasions, local-scale wind has been associated with freezing precipitation phenomena [*Henson et al.*, 2011]. Terrain-driven convergence can occur in mountain systems when there are weak winds perpendicular to the barrier [*Kim and Kang*, 2007; *Rowe et al.*, 2012], which is linked to freezing precipitation [*Hughes et al.*, 2012].

When there is a preexisting layer of cold air at the surface, a warm and moist air mass must first ascend over this layer [*Houze*, 2012]. Cold air accumulated at low levels could not cross the mountain range owing to its higher density and therefore flowed parallel to the barrier. However, warm air at midlevels did cross the mountains. The result was the formation of a narrow orographic cloud layer under the warm air mass, which led to the development of freezing drizzle.

The image at 15:00 UTC shows that as the cold air mass approached, the wind shifted to a northerly component and increased in strength, so it could easily traverse the barrier. Throughout the day, wind perpendicular to the orographic barrier formed a mesolow downwind, as observed by *Fernández-González et al.* [2014a] during a similar episode.

4.2. Hourly Precipitation

Figure 6 shows hourly precipitation at three defining moments on the study day. First, the image at 09:00 UTC indicates weak precipitation as a result of the warm, moist air mass rising over the cold air mass persisting upwind of the orographic barrier. The Guadarrama Mountains caused orographic enhancement, as evidenced by the greater amount of precipitation modeled by the WRF around the mountain peaks and windward slopes, similar to that described by *Banfield et al.* [2000]. In a blocked flow case, air is forced to rise before reaching the barrier [*Medina and Houze*, 2003], causing precipitation intensification upwind of the mountains. At Navacerrada Pass, this precipitation was in the form of light snow.

At 12:00 UTC, the cold air mass arrived from northeast of D04, causing moderate precipitation. In the prefrontal area, weak precipitation was produced upwind of the Guadarrama Mountains, which may be connected with

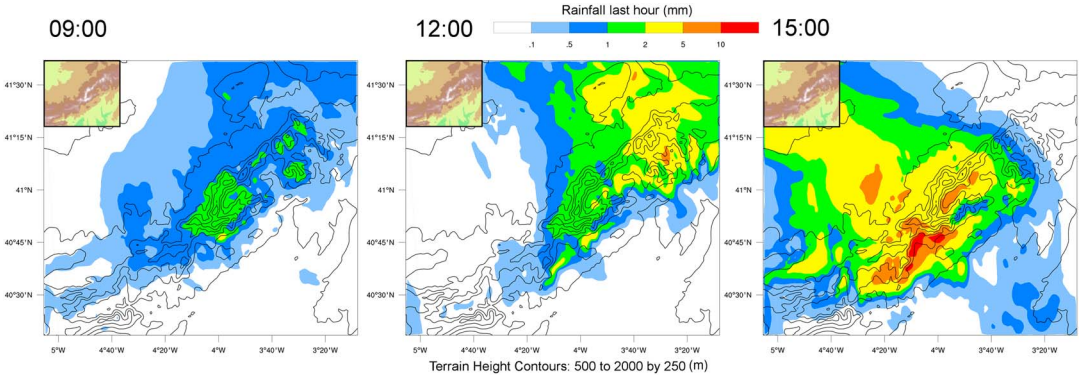

Figure 6. Hourly precipitation in millimeters, estimated by WRF for D04. Orography is underlain and shown in the top left.

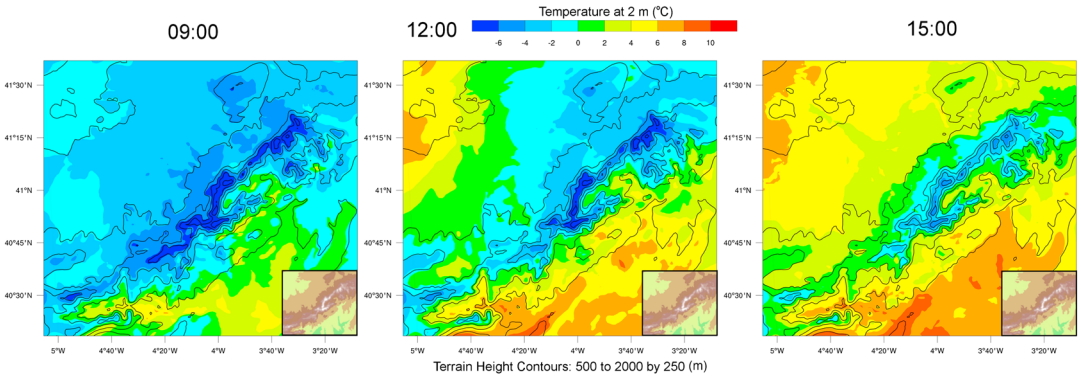

Figure 7. Temperature (°C) at 2 m above the surface, modeled by WRF in D04. Orography is underlain and shown in the bottom right.

freezing precipitation in the same icing event described by *Fernández-González et al.* [2014b]. As in the present event, *Zhou et al.* [2013] observed intensities around 0.5 mm h^{-1} during a freezing drizzle episode.

Following a northeast-southwest trajectory, precipitation with arrival of the cold air mass began to affect the study area at 15:00 UTC, causing moderate precipitation as snow at high altitudes of the Guadarrama Mountains. This concurs with *Woods et al.* [2005], who noted that precipitation intensity increases as a cold air mass approaches an orographic barrier. Downslope flow on the leeward side, which originated from wind perpendicular to the barrier, produced a local rain shadow because of the Foehn effect, thereby weakening penetration of the cold air mass downwind of the mountain range. This resulted in almost no precipitation on the south side of those mountains for the remainder of the day.

4.3. Surface Temperature

Figure 7 shows surface temperature on 5 February 2012. At 09:00 UTC, effects of the continental polar air mass present during the last few days could still be seen. Given the low modeled temperatures in the mountains and to the north, a thermal inversion formed during nighttime could also have contributed to these low temperatures. South of the mountain chain, temperatures were warmer as a result of the Foehn effect, exceeding 0°C at lower altitudes. It is common that freezing precipitation episodes are preceded by temperatures near −10°C [*Eriksson*, 2001].

The rise in temperature observed at 12:00 UTC is consistent with arrival of the warm air mass. This was most noticeable in the northwestern part of D04, where the air mass originated. However, temperatures remained low on the north side of the Guadarrama Mountains, consistent with cold air damming. This prevented the warm air mass from affecting the surface, which maintained subzero temperatures on the north side of the mountains, essential for the production of freezing drizzle. At Navacerrada Pass, surface temperature increased slightly in the hours before the freezing drizzle onset, although it failed to rise above 0°C. Our results are similar to those of *Carrière et al.* [2000], who observed that most freezing precipitation events have surface temperatures between −5°C and 0°C. Freezing drizzle in areas with subzero temperatures can produce local increases in surface temperature, because latent heat is released during the freezing process [*Lackmann et al.*, 2002]. If there is no cold air advection, this process tends to raise surface temperatures, up to 0°C. *Cortinas* [2000] observed that for this reason, only 10% of freezing drizzle episodes last more than 5 h. In our case, since the initial temperature was very low (around −7°C) and freezing precipitation intensity was weak ($\sim$ 1 mm h^{-1}), the latent heat release appears to have been insufficient to raise surface temperatures above freezing, thereby facilitating the freezing drizzle that lasted $\sim$ 2 h.

In the afternoon (15:00 UTC), subfreezing temperatures were restricted to high elevations, because the advancing cold air mass dissipated the thermal inversion; this may have also been affected by solar heating. Snow cover at higher altitudes (above 1750 m asl) in the Guadarrama Mountains [*Fernández-González et al.*, 2014b] may have helped maintain subfreezing surface temperatures there throughout the day.

4.4. Updrafts

Figure 8 displays vertical wind velocity modeled in D04. During the entire day the WRF detected a weak updraft upwind of the mountain, but one strong enough to generate low orographic clouds. The wind flow

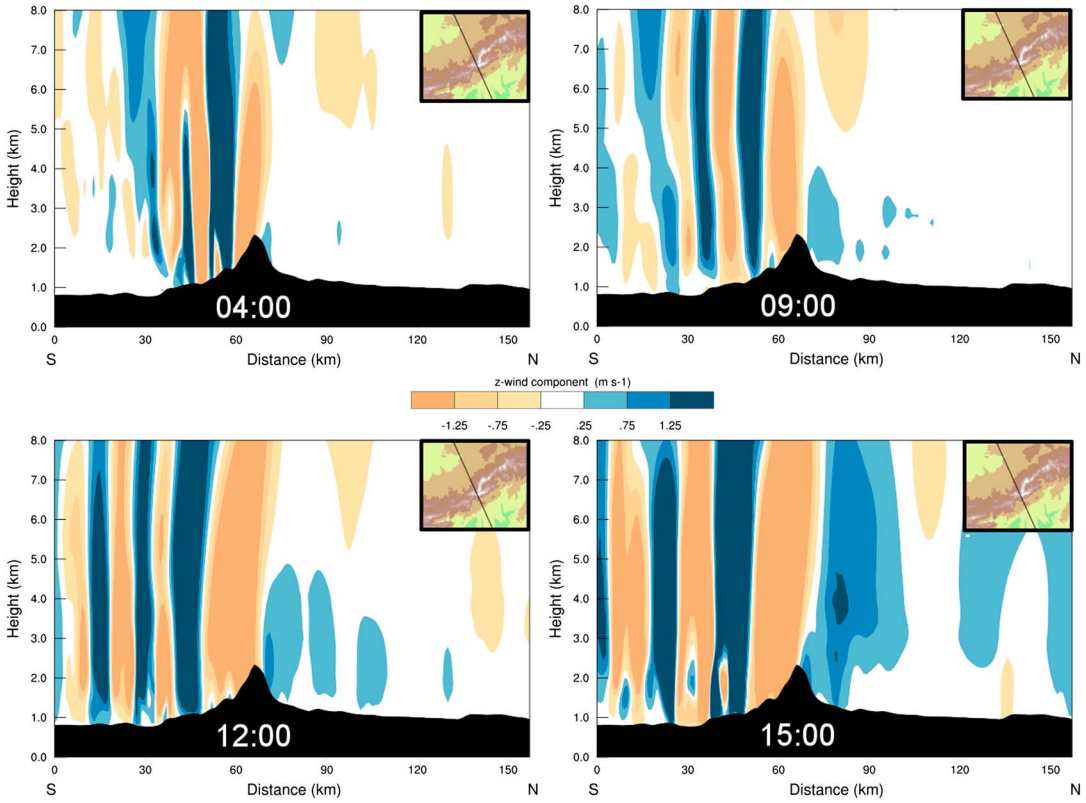

Figure 8. Cross section of vertical wind speed (m s^{-1}) in D04. Underlying orography is shown in solid black. Direction of cross section is shown in the top right.

perpendicular to the Guadarrama Mountains may have been the cause of this updraft, consistent with *Kim and Kang* [2007]. This updraft did not reach 4000 m asl during the first hours of the day (images of 04:00 and 09:00 UTC) because it was within a stable layer that prevented vertical cloud development. A downdraft was generated downwind of the mountains, linked to the Foehn effect. Further southeast, there were alternating updrafts and downdrafts, which increased in intensity as the day progressed and wind speed intensified; this pattern was likely caused by mountain waves.

The image at 12:00 UTC, which coincides with the freezing drizzle event, clearly shows the updraft upwind of the mountains. As the cold air mass approached, this flow intensified and increased in vertical extent. Updraft intensification favors increased efficiency of collision and coalescence processes, enabling drizzle to form rapidly [*Geresdi and Rasmussen*, 2005]. The development of freezing drizzle is frequently associated with gradual lifting of air masses along the slopes of orographic barriers [*Bernstein*, 2000; *Cortinas et al.*, 2004]. Our results agree with those of *Rasmussen et al.* [1995], who analyzed a freezing drizzle episode caused by the uplift of air with magnitude ~ 0.1 m s^{-1} over an arctic front.

At 16:00 UTC there was updraft intensification north of the Guadarrama Mountains, even exceeding 1 m s^{-1} between 3 and 5 km elevation. It is possible that this intensification was caused by the arrival of the cold air mass and strengthened by orographic lift, generating increased LWC and intense riming of ice particles precipitated at upper levels, as described by *Viale et al.* [2013].

4.5. Atmospheric Stability

To analyze atmospheric stability, we constructed a cross section of θ_e gradient ($d\theta_e$) in Figure 9. This indicates whether conditions in the troposphere are stable ($d\theta_e > 0$), neutral ($d\theta_e = 0$), or unstable ($d\theta_e < 0$) [*Wang*, 2013]. At dawn and throughout the morning, there was a stable layer at the surface that persisted until the cold air mass arrival after midday. At 04:00 UTC the atmospheric stability dominated almost the entire troposphere, with only a small unstable layer upwind of the Guadarrama Mountains, which enabled development of orographic clouds in this area. The image at 09:00 UTC reveals a stable layer in the first few hundred meters above the surface, probably associated with the continental polar cold and dry air mass.

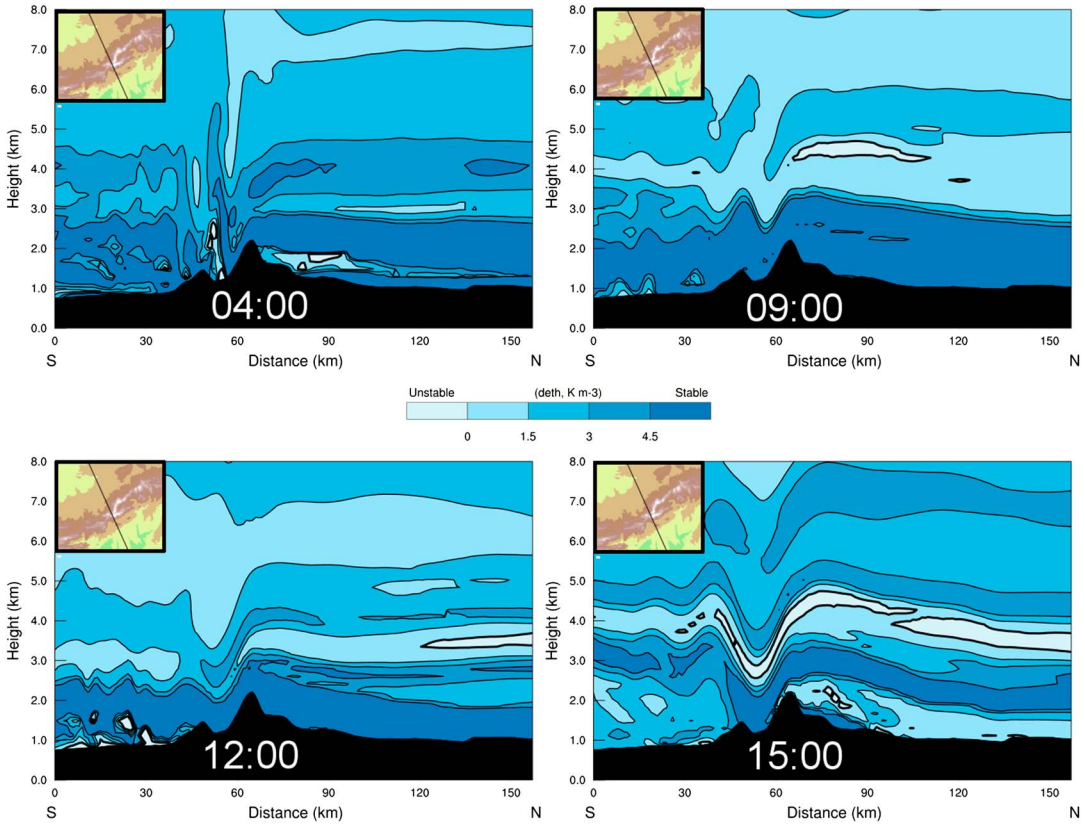

Figure 9. Cross section of $d\theta_e$(K m^{-3}) in D04. Underlying orography is shown in solid black. Direction of cross section is shown in the top left.

When low-level winds are blocked by an orographic barrier, a low-level stable layer is produced upwind [*Houze*, 2012]. The warm, moist air mass was forced to ascend over this layer, resulting in a potentially unstable layer between 3000 and 5000 m asl, which facilitated the development of clouds in this layer.

At 12:00 UTC, the potentially unstable layer at midlevels had practically disappeared. At this time, atmospheric stability prevailed over the Guadarrama Mountains, even extending above 5000 m asl, which impeded midlevel cloud formation. A stable layer prevented cloud vertical development, maintaining relatively warm cloud top temperatures and impeding ice crystal formation. Atmospheric stability prevailed within the boundary layer throughout the morning. Therefore, at this time there were only orographic clouds on the north side of the mountains, which caused the freezing drizzle. This is consistent with *Pobanz et al.* [1994], who pointed out that neutral static stability, together with weak updrafts linked to orography, might be associated with the generation of supercooled liquid water.

Subsequently (15:00 UTC), there was increased instability at low levels, which triggered dissipation of the surface inversion. Increased instability was also observed between 3000 and 4500 m asl. This was consistent with wedge-shaped entry of the cold air mass, which forced the warm, moist air mass upward, as described by *Hanesiak and Stewart* [1995]. With approach of the cold air mass, increased wind speed caused a shift to unblocked flow (see Figure 5), which increased instability in the study area. In short, near-neutral conditions prevailed throughout the day, with greater instability during arrival of the warm, moist air mass and approach of the cold air mass.

4.6. Cross Section of Relative Humidity and Temperature

Vertical structure of temperature and RH in the first 8 km of the troposphere is shown in Figure 10, via a cross section of D04 that traverses Navacerrada Pass. At dawn (image at 04:00 UTC), moisture accumulation is seen in the first few meters on the upwind slope of the Guadarrama Mountains, which aided development of low orographic clouds with reduced thickness. There was no precipitation recorded at this time. At 09:00 UTC

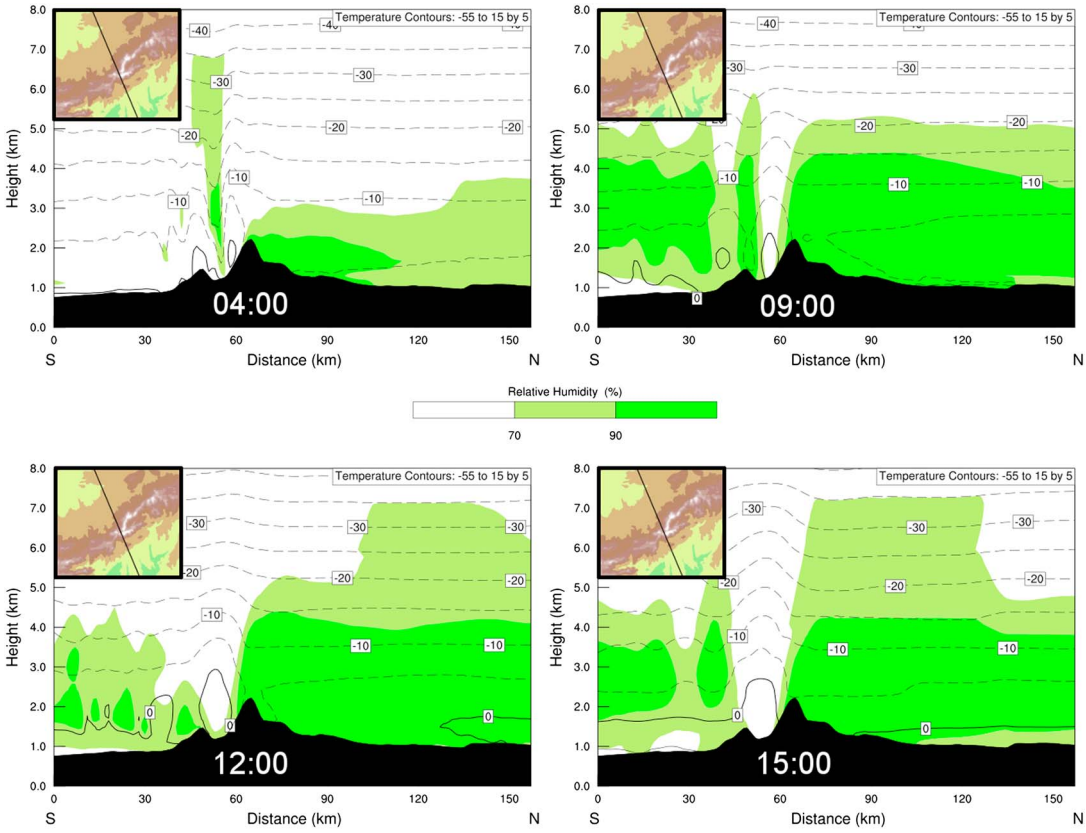

Figure 10. Cross section of RH (shaded, in percent) and temperature (contours, in °C) in D04. Underlying orography is shown in solid black. Direction of cross section is shown in the top left.

increased moisture can be seen, even reaching the −20°C isotherm because of the entrance of the moist and warm air mass. This allowed a greater vertical development of cloudiness.

At the time of freezing drizzle initiation (12:00 UTC), the warm and moist air mass-induced moisture near saturation in the first 4000 m asl, such that the cloud top temperature was about −15°C. RH was low above the level of the −20°C isotherm (< 70%), indicating no saturation with respect to ice. *Korolev et al.* [2003] noted that at temperatures warmer than −15°C, LWC predominates over Ice Water Content (IWC), suggesting that the orographic cloud was mainly in liquid phase at this time. North of the Guadarrama Mountains, RH >70% extended to 7 km, which appeared to be a prelude to arrival of the cold air mass. This moisture flow over inland terrain gave rise to orographic clouds on the windward side of the mountains.

The image at 15:00 UTC shows increased RH just ahead of the cold air mass, with values > 70% reaching even above the level of the −30°C isotherm. This facilitated development of midlevel clouds and enabled glaciation processes, with cloud top temperatures below −20°C. These clouds were likely mainly in solid phase. During the day, we observed that at a given altitude, temperatures were markedly higher on the southern slopes. In addition, an area of low moisture is seen downwind of the mountain range. Both these phenomena are probable consequences of the Foehn effect. By contrast, RH upwind was near saturation throughout the study period and the maximum WRF temperature forecast for Navacerrada was less than 0°C, making possible the freezing drizzle. These results agree with those of *Chen et al.* [2011].

4.7. Liquid and Ice Water Content

Figure 11 displays LWC and IWC estimated by WRF on a cross section of D04. At dawn (image at 04:00 UTC), wind perpendicular to the Guadarrama Mountains produced orographic clouds on the northern slopes, owing to moisture retention by the mountain range. At this time, the small vertical extent of the clouds and low LWC prevented precipitation formation, although these conditions led to in-cloud icing as described below. This cloud layer of variable thickness, and LWC dependent on the moisture supply and updraft intensity, persisted

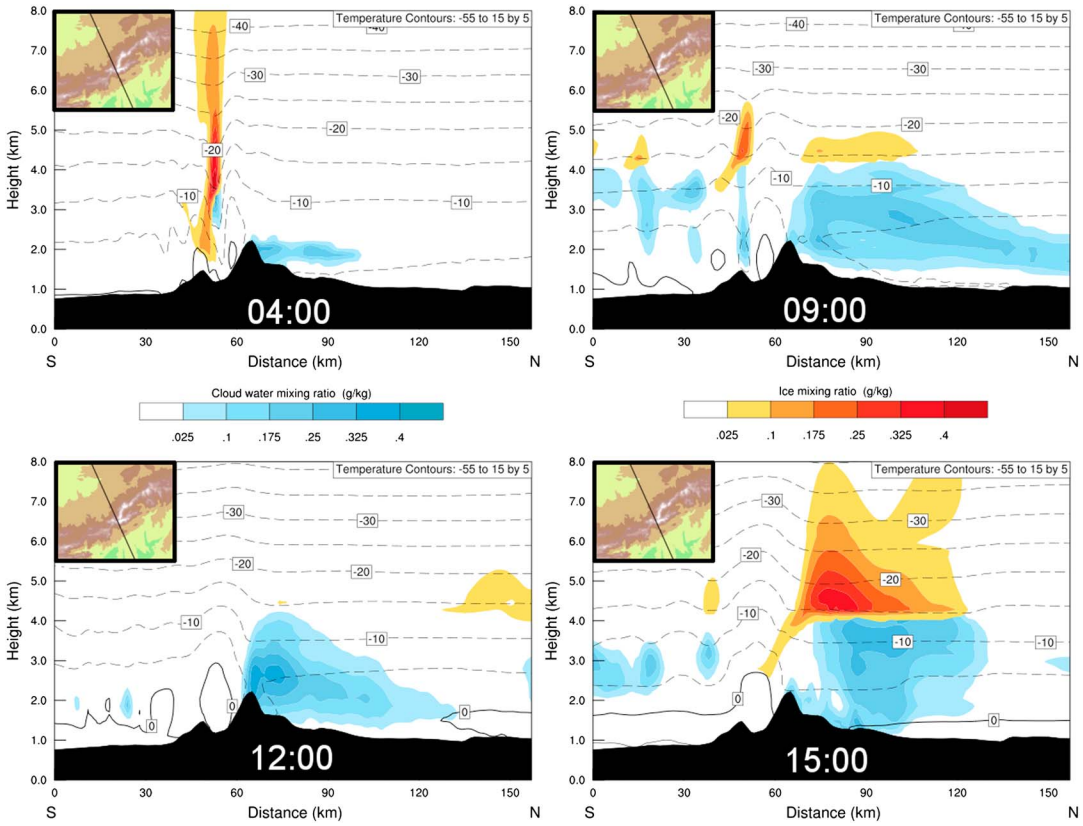

Figure 11. Cross section of LWC (g kg^{-1}), IWC (g kg^{-1}), and temperature (contours, in °C) in D04. Underlying orography is shown in solid black. Direction of cross section is shown in the top left.

in the study area throughout the study period. An area of clouds was observed downwind, probably caused by the Foehn effect.

The image at 09:00 UTC shows increased LWC in the first 4 km of the troposphere and solid-phase clouds at midlevels. This situation was probably the result of the warm air mass reaching the mountains, being forced to rise there above the cold air mass. Stable updrafts originating from moisture advection produced orographic clouds. These clouds were then fed by hydrometeors generated by precipitation falling from a higher seeder cloud aloft, which was produced by uplift along a warm air conveyor, consistent with *Sibley* [2005].

At 12:00 UTC, there was a considerable increase of cloud top temperature. This may be attributable to decreased RH and increased stability at midlevels. With orographic cloud top temperatures warmer than −15°C, development of glaciation was inhibited and the seeder cloud dissipated. Thus, it is likely that nearly all hydrometeors within the clouds were in a liquid state. Because the wind flow was perpendicular to the orographic barrier and low-level moisture remained high, the orographic clouds persisted.

Surface temperatures colder than 0°C enabled development of freezing drizzle. The elevated LWC (up to 0.35 g kg^{-1}) of the orographic cloud favored drizzle formation via collision-coalescence processes. WRF indicated that temperature in the upper region of the cloud was −15°C, with low ice crystal concentrations. Previous studies have described the generation of freezing drizzle in clouds associated with weak uplift, low ice crystal concentration, warm cloud tops, and stably stratified conditions [*Marwitz et al.*, 1997; *Bernstein et al.*, 1998; *Bernstein*, 2000]. At 12:00 UTC, the efficiency of the collision-coalescence processes increased together with orographic cloud layer thickness, as described by *Kajikawa et al.* [2000], allowing the supercooled drops to grow to drizzle size and thereby favoring precipitation. Subsequent drying after passage of the humid air mass in the midtroposphere caused a cessation of the seeder ice crystals that had previously fallen through the lower layers and riming there, preventing the formation of supercooled precipitation, as in the case analyzed by *Juga et al.* [2012].

Table 1. Freezing Drizzle Accumulation Estimated by WRF as Function of a Given IWP Limit

IWP Limit ($g\ m^{-2}$)	Freezing Drizzle (mm)	
	Forecast	Observed
0.1	1.0	2
0.5	1.5	2
1.0	2.0	2
2.0	2.5	2
5.0	4.0	2

In the image at 15:00 UTC, clouds are seen even above the −20°C isotherm level, probably because the cold air mass began to affect the study area by causing moisture advection, instability at midlevels, and increased updraft intensity, factors that favor development of glaciation. The increased LWC in the orographic cloud created optimal conditions for development of the seeder-feeder process [*Iguchi et al.*, 2012]. Ice crystal growth by vapor diffusion and riming is more efficient than water collection by rainfall [*Choularton and Perry*, 1986], such that when a seeder-feeder mechanism is produced, precipitation intensity increases. These processes intensified at 15:00 UTC, when the updrafts were strongest.

Moisture and upslope flow facilitate the coexistence of liquid- and solid-phase clouds, which favor the seeder-feeder process and thereby increase the amount of accumulated precipitation, consistent with *Saleeby et al.* [2009]. Finally, the greatest vertical cloud development at midlevels just upstream of the Guadarrama Mountains indicates orographic enhancement, which enabled formation of additional ice particles.

4.8. Freezing Drizzle

Conventional outputs of the principal numerical weather prediction models do not include the detection of freezing precipitation, so there is great uncertainty when forecasting this meteorological phenomenon. We therefore determined freezing drizzle accumulation by combining the WRF outputs of precipitation, surface temperature, and ice water path (IWP). This algorithm calculates the accumulation of freezing drizzle in areas where expected surface temperature is < 0°C and IWP $< 1\ g\ m^{-2}$. Several studies [*Rasmussen et al.*, 1995; *Cober et al.*, 2001; *Geresdi et al.*, 2005] determined that if ice concentration is $< 0.1\ L^{-1}$, precipitation will likely be in liquid form. A value of IWP $< 1\ g\ m^{-2}$ was empirically determined after comparing algorithm results with observations at Navacerrada Pass (Table 1). The IWP limit should be revised if this algorithm is applied to another region. This approach is only valid for forecasting freezing precipitation originating from the warm rain process. However, the approach may not detect freezing precipitation events caused by melting of ice crystals upon traversing a layer with temperatures warmer than 0°C, followed by a thermal inversion layer, with temperatures colder than 0°C at the surface.

During the morning (image at 09:00 UTC of Figure 12), the entry of the moist air mass and instability at midlevels gave rise to the development of nucleation processes, with IWP $> 1\ g\ m^{-2}$, such that the algorithm did not identify any accumulation of freezing drizzle. This coincides with the observation of light snow throughout the morning.

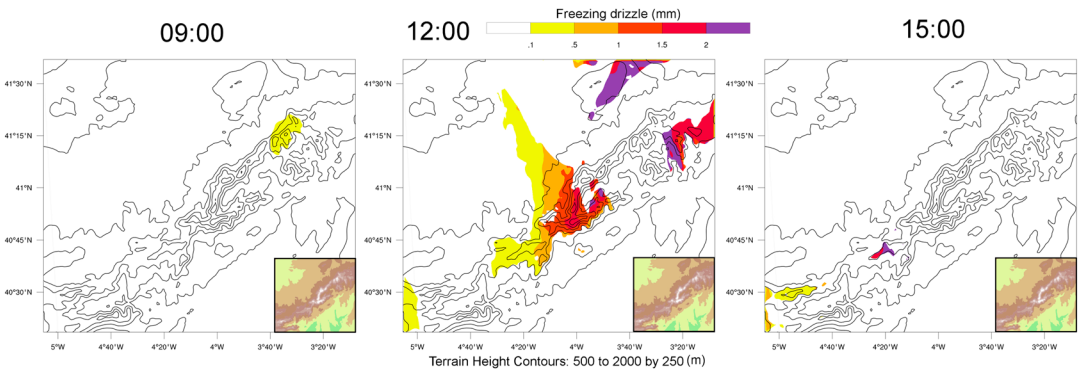

Figure 12. Hourly freezing drizzle (mm) estimated by WRF for D04. Orographic contours are underlain and orography is also shown in the bottom right.

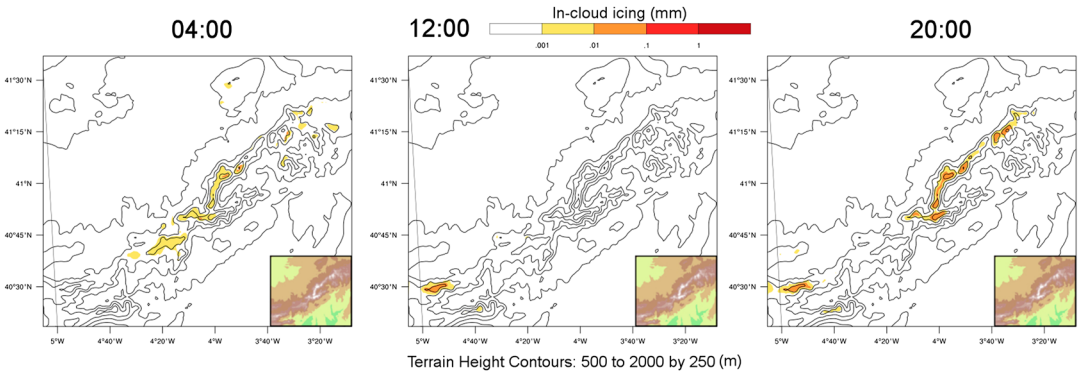

Figure 13. Hourly in-cloud icing (mm) estimated by WRF for D04. Orographic contours are underlain and orography is also shown in the bottom right panels.

As evident in Figure 12, the algorithm identified freezing drizzle before entry of the cold air mass (image at 12:00 UTC). Specifically, the algorithm simulated between 1 and 2 mm h^{-1} of freezing drizzle, which agrees with the observations [*Fernández-González et al.*, 2014b]. During the prefrontal period, the combination of the loss of seeder cloud aloft and prevalence of warm, moist low-level cloud permitted drizzle drops to form, as observed *Ikeda et al.* [2007]. The fact that the cloud top temperature was warmer than −15°C at this time hampered proper development of the glaciation process, thereby favoring clouds that were almost entirely in liquid phase. The very low concentration of active ice nuclei at these temperatures [*Rosenfeld et al.*, 2013] could be a major reason for the shortage of ice crystals in the cloud that produced the freezing drizzle.

At 15:00 UTC, the cold air mass increased the IWP, thereby inhibiting the generation of freezing drizzle, which was restricted to the western D04 where its effects were not yet noticeable. Falling ice crystals from upper levels could deplete supercooled cloud droplets via deposition and riming, inhibiting precipitation in the form of freezing drizzle because of elevated collection efficiency of supercooled drops by ice crystals, consistent with *Pruppacher and Klett* [1997].

As in the event analyzed, it is common for freezing drizzle to alternate with snowfall [*Roberts and Stewart*, 2008]. This makes it important to determine the type of expected precipitation at all times, because the risks and effects of each meteorological phenomenon vary.

4.9. In-Cloud Icing

Meteorological conditions favorable for in-cloud icing are well defined: LWC at the surface (which occurs when the cloud base is below the location of observation), high wind speeds, and subfreezing surface temperatures [*Makkonen and Lozowski*, 2008]. We developed an application to detect in-cloud icing, as follows. First, areas with surface temperatures warmer than 0°C were eliminated, since these have no accumulation of in-cloud icing. In the remaining areas with subzero temperatures, the amount of expected in-cloud icing was calculated by multiplying LWC by surface wind speed, thereby obtaining the in-cloud icing rate in mm h^{-1}.

As shown in Figure 13, this application detected in-cloud icing during the early morning and late evening (images at 04:00 and 20:00 UTC). During this period, wind perpendicular to the Guadarrama Mountains pooled moisture on the windward slopes, forming low orographic clouds presumably in liquid phase, owing to cloud top temperatures warmer than −15°C. Since their thickness and LWC were moderate, these clouds did not produce precipitation. However, these did cause in-cloud icing because the cloud base was below the highest elevations of the Guadarrama Mountains, where the algorithm detected in-cloud icing. Nevertheless, in-cloud icing rates were so low that they did not cause any major problems.

The image at 04:00 UTC (Figure 11) shows that the base of the orographic cloud was below Navacerrada Pass. The largest amounts of LWC were around the top of the pass, around 0.25 g kg^{-1}. LWC in our study was considerable compared with the concentrations observed by *Podolskiy et al.* [2012], although perhaps the weak wind at 04:00 UTC was the reason for lack of severe in-cloud icing, as described by *Drage and Thiis* [2013]. This methodology may be useful for mountain ranges exposed to strong and moist winds, where in-cloud icing could be a serious problem.

5. Concluding Remarks

The freezing drizzle and seeder-feeder episodes in the Guadarrama Mountains on 5 February 2012 arose from a combination of factors. In the early morning hours, a continental cold and dry air mass was situated over the Iberian Peninsula. Northwesterly winds supplied moisture, which was retained upwind of the mountain range, forming low orographic clouds. Low LWC and thickness of these clouds did not permit hydrometeors to grow sufficiently large to result in precipitation. However, modeling indicated that in-cloud icing may have occurred.

During the morning, an oceanic air mass arrived from the Atlantic, which was warmer and moister. The ascent of this air mass over preexisting cold air over the peninsula triggered increased instability and an increase of cloud thickness, reaching cloud top temperatures around −20°C. This enabled development of glaciation processes, generating ice crystals that underwent riming upon passing through supercooled large drops in the orographic cloud and producing light snow at the surface.

Subsequent entry of drier and more stable air at mid levels of the troposphere increased cloud top temperatures to warmer than −15°C. The orographic barrier caused a blocking situation because of weak winds at the surface, which generated flow parallel to the mountain range and moisture accumulation upwind of it. Together with weak updrafts caused by the orography, this increased the efficiency of collision-coalescence processes and formed supercooled large drops that produced freezing drizzle.

Finally, the arrival of a cold air mass triggered moisture advection and instability at midlevels. Increased wind speed destroyed the blocking and increased vertical extent and updraft intensity. These phenomena caused clouds with temperatures less than −20°C, which reinitiated the glaciation. A seeder cloud formed, which produced ice crystals above the low-level feeder cloud via the seeder-feeder mechanism. This prevented the fall of freezing drizzle and caused moderate snowfall at Navacerrada Pass.

In summary, we stress that in the study of freezing precipitation, analysis of mesoscale meteorological factors is fundamental. When there are multiple cloud layers, cloud top temperature at various levels and distance between levels are the most important factors that determine the type of precipitation reaching the surface.

Acknowledgments

Data support was from the Atmospheric Physics Group, IMA, University of León, Spain. To request the data, please contact S. Fernández-González (sefern04@ucm.es). This paper was supported by the following grants: TEcoAgua, METEORISK PROJECT (RTC-2014-1872-5), Granimetro (CGL2010-15930) and CGL2011-25327 of MINECO, and LE220A11-2 and LE003B009 awarded by the Junta de Castilla y León. Special thanks to Roberto Weigand, Ángel Guerrero, Steven Hunter, and Analisa Weston. We thank Canal de Isabel II Gestion for use of their facilities. S. Fernández-González acknowledges grant the support from the FPU program (AP 2010-2093).

References

Banfield, C. E., D. R. Hudak, and A. D. Thomson (2000), Orographic influences during winter precipitation events on the Avalon Peninsula, Newfoundland, *Meteorol. Appl.*, *7*, 297–311.

Bernstein, B. C. (2000), Regional and local influences on freezing drizzle, freezing rain and ice pellet events, *Weather Forecasting*, *15*, 485–508, doi:10.1175/1520-0434(2000)015<0485:RALIOF>2.0.CO;2.

Bernstein, B. C., T. A. Omeron, M. K. Politovich, and F. McDonough (1998), Surface weather features associated with freezing precipitation and severe in-flight aircraft icing, *Atmos. Res.*, *46*, 57–73, doi:10.1016/S0169-8095(97)00051-3.

Browning, K. A. (1997), The dry intrusion perspective of extra-tropical cyclone development, *Meteorol. Appl.*, *4*, 317–324.

Carrière, J. M., S. Alquier, C. L. Bot, and E. Moulin (1997), Statistical verification of forecast icing risk indices, *Meteorol. Appl.*, *4*, 115–130, doi:10.1017/S1350482797000443.

Carrière, J. M., C. Lainard, C. L. Bot, and F. Robart (2000), A climatological study of surface freezing precipitation in Europe, *Meteorol. Appl.*, *7*, 229–238.

Castellano, N. E., E. E. Avila, and C. P. R. Saunders (2004), Theoretical model of the Bergeron-Findeisen mechanism of ice crystal growth in clouds, *Atmos. Environ.*, *38*, 6751–6761, doi:10.1016/j.atmosenv.2004.09.003.

Chen, B., W. Hu, and J. Pu (2011), Characteristics of the raindrop size distribution for freezing precipitation observed in Southern China, *J. Geophys. Res.*, *116*, D06201, doi:10.1029/2010JD015305.

Chen, F., and J. Dudhia (2001), Coupling an advanced land surface-hydrology model with the Penn State-NCAR MM5 modeling system. Part I: Model implementation and sensitivity, *Mon. Weather Rev.*, *129*, 569–585.

Choularton, T. W., and S. J. Perry (1986), A model of the orographic enhancement of snowfall by the seeder-feeder mechanism, *Q. J. R. Meteorol. Soc.*, *112*, 335–345.

Cober, S. G., J. W. Strapp, and G. A. Isaac (1996), An example of supercooled drizzle drops formed through a collision-coalescence process, *J. Appl. Meteorol.*, *35*, 2250–2260, doi:10.1175/1520-0450(1996)035<2250:AEOSDD>2.0.CO;2.

Cober, S. G., G. A. Isaac, and J. W. Strapp (2001), Characterizations of aircraft icing environments that include supercooled large drops, *J. Appl. Meteorol.*, *40*, 1984–2002, doi:10.1175/1520-0450(2001)040<1984:COAIET>2.0.CO;2.

Cortinas, J. (2000), A climatology of freezing rain in the Great Lakes region of North America, *Mon. Weather Rev.*, *128*, 3574–3588, doi:10.1175/1520-0493(2001)129<3574:ACOFRI>2.0.CO;2.

Cortinas, J. V., B. C. Bernstein, C. C. Robbins, and J. W. Strapp (2004), An analysis of freezing rain, freezing drizzle, and ice pellets across the United States and Canada: 1976–90, *Weather Forecasting*, *19*, 377–390, doi:10.1175/1520-0434(2004)019<0377:AAOFRF>2.0.CO;2.

Drage, M., and G. Hauge (2007), Atmospheric icing in a coastal mountainous terrain. Measurements and numerical simulations, a case study, *Cold Reg. Sci. Technol.*, *53*, 150–161, doi:10.1016/j.coldregions.2007.12.003.

Drage, M. A., and T. K. Thiis (2013), Large-scale measurements and numerical simulations of in-cloud icing around a mountain ridge, *J. Wind Eng. Ind. Aerodyn.*, *104*, 523–531, doi:10.1016/j.jweia.2012.02.028.

Dudhia, J. (1989), Numerical study of convection observed during the Winter Monsoon Experiment using a mesoscale two-dimensional model, *J. Atmos. Sci.*, *46*, 3077–3107, doi:10.1175/1520-0469(1989)046<3077:NSOCOD>2.0.CO;2.

Erfani, R., L. Chouinard, and L. Cloutier (2014), De-aggregated hazard of freezing rain events, *Atmos. Res.*, *145-146*, 297–312, doi:10.1016/j.atmosres.2014.03.024.

Eriksson, M. (2001), Regional influence on the occurrence of road slipperiness during winter precipitation events, *Meteorol. Appl.*, *8*, 449–460, doi:10.1017/S1350482701004066.

Fargey, S., W. Henson, J. Hanesiak, and R. Goodson (2014), Characterization of an unexpected snowfall event in Iqaluit, Nunavut, and surrounding area during the Storm Studies in the Arctic field project, *J. Geophys. Res. Atmos.*, *119*, 5492–5511, doi:10.1002/2013JD021176.

Fernández-González, S., J. L. Sánchez, E. Gascón, L. López, E. García-Ortega, and A. Merino (2014a), Weather features associated with aircraft icing conditions: A case study, *Sci. World J.*, *279063*, 1–18, doi:10.1155/2014/279063.

Fernández-González, S., F. Valero, J. L. Sánchez, E. Gascón, L. López, E. García-Ortega, and A. Merino (2014b), Observation of a freezing drizzle episode: A case study, *Atmos. Res.*, *149*, 244–254, doi:10.1016/j.atmosres.2014.06.014.

Fikke, S. M., J. E. Kristjansson, and B. E. K. Nygaard (2008), Modern meteorology and atmospheric icing, *Atmos. Icing Power Networks*, *2008*, 1–29, doi:10.1007/978-1-4020-8531-4_1.

Gascón, E., J. L. Sánchez, D. Charalambous, S. Fernández-González, L. López, E. García-Ortega, and A. Merino (2015), Numerical diagnosis of a heavy snowfall event in the center of the Iberian Peninsula, *Atmos. Res.*, *153*, 250–263, doi:10.1016/j.atmosres.2014.08.001.

Geresdi, I., and R. Rasmussen (2005), Freezing drizzle formation in stably stratified layer clouds. Part II: The role of giant nuclei and aerosol particle size distribution and solubility, *J. Atmos. Sci.*, *62*, 2037–2057, doi:10.1175/JAS3452.1.

Geresdi, I., R. Rasmussen, W. Grabowski, and B. Bernstein (2005), Sensivity of freezing drizzle formation in stably stratified clouds to ice processes, *Meteorol. Atmos. Phys.*, *88*, 91–105, doi:10.1007/s00703-003-0048-5.

Gross, B. D. (1994), Frontal interaction with isolated orography, *J. Atmos. Sci.*, *51*, 1480–1496.

Hanesiak, J. M., and R. E. Stewart (1995), The mesoscale and microscale structure of a severe ice pellet storm, *Mon. Weather Rev.*, *123*, 3144–3162.

Heimann, D. (1992), Potential and equivalent-potential temperature patterns at cold fronts with prefrontal Foehn, *Meteorol. Atmos. Phys.*, *48*, 165–171.

Henson, W., R. Stewart, and B. Kochtubajda (2007), On the precipitation and related features of the 1998 ice storm in the Montreal area, *Atmos. Res.*, *83*, 36–54, doi:10.1016/j.atmosres.2006.03.006.

Henson, W., R. Stewart, B. Kochtubajda, and J. Theriault (2011), The 1998 ice storm: Local flow fields and linkages to precipitation, *Atmos. Res.*, *101*, 852–862, doi:10.1016/j.atmosres.2011.05.014.

Hewson, T. D. (1998), Objective fronts, *Meteorol. Appl.*, *5*, 37–65.

Hosek, J., P. Musilek, E. Lozowski, and P. Pytlak (2011), Forecasting severe ice storms using numerical weather prediction: The March 2010 Newfoundland event, *Nat. Hazards Earth Syst. Sci.*, *11*, 587–595, doi:10.5194/nhess-11-587-2011.

Houze, R. A. (2012), Orographic effects on precipitating clouds, *Rev. Geophys.*, *50*, RG1001, doi:10.1029/2011RG000365.

Hughes, M., P. J. Neiman, E. Sukovich, and M. Ralph (2012), Representation of the Sierra Barrier Jet in 11 years of a high-resolution dynamical reanalysis downscaling compared with long-term wind profiler observations, *J. Geophys. Res. Atmos.*, *117*, D18116, doi:10.1029/2012JD017869.

Iguchi, T., T. Matsui, J. J. Shi, W. K. Tao, A. P. Khain, A. Hou, R. Cifelli, A. Heymsfield, and A. Tokay (2012), Numerical analysis using WRF-SBM for the cloud microphysical structures in the C3VP field campaign: Impacts of supercooled droplets and resultant riming on snow microphysics, *J. Geophys. Res. Atmos.*, *117*, D23206, doi:10.1029/2012JD018101.

Ikeda, K., R. M. Rasmussen, W. D. Hall, and G. Thompson (2007), Observations of freezing drizzle in extratropical cyclonic storms during IMPROVE-2, *J. Atmos. Sci.*, *64*, 3016–3043, doi:10.1175/JAS3999.1.

Janjic, Z. (1996), *The Surface Layer Parameterization in the NCEP Eta Model*, 444 pp., World Meteorol. Organ. Publ., Geneva, Switzerland.

Jenkner, J., M. Sprenger, I. Schwenk, C. Schwierz, S. Dierer, and D. Leuenberger (2010), Detection and climatology of fronts in a high-resolution model reanalysis over the Alps, *Meteorol. Appl.*, *17*, 1–18, doi:10.1002/met.142.

Juga, I., M. Hippi, D. Moisseev, and E. Saltikoff (2012), Analysis of weather factors responsible for the traffic Black Day in Helsinki, Finland, on 17 March 2005, *Meteorol. Appl.*, *19*, 1–9, doi:10.1002/met.238.

Kajikawa, M., K. Kikuchi, Y. Asuma, Y. Inoue, and N. Sato (2000), Supercooled drizzle formed by condensation-coalescence in the mid-winter season of the Canadian Arctic, *Atmos. Res.*, *52*, 293–301, doi:10.1016/S0169-8095(99)00035-6.

Kim, J., and H. S. Kang (2007), The impact of the Sierra Nevada on low-level winds and water vapor transport, *J. Hydrometeorol.*, *8*, 790–804, doi:10.1175/JHM599.1.

Korolev, V., G. A. Isaac, S. G. Cober, J. W. Strapp, and J. Hallett (2003), Observation of the microstructure of mixed phase clouds, *Q. J. R. Meteorol. Soc.*, *129*, 39–66, doi:10.1256/qj.01.204.

Laakso, T., I. Baring-Gould, M. Durstewitz, R. Horbaty, A. Lacroix, E. Peltola, G. Ronsten, L. Tallhaug, and T. Wallenius (2010), *State of the Art of Wind Energy in Cold Climates*, p. 152, VTT Tech. Res. Cent. Finland, Esbo, Finland.

Lackmann, G. M., K. Keeter, L. G. Lee, and M. B. Ek (2002), Model representation of freezing and melting precipitation: Implications for winter weather forecasting, *Weather Forecasting*, *17*, 1016–1033, doi:10.1175/1520-0434(2003)017<1016:MROFAM>2.0.CO;2.

Lamraoui, F., G. Fortin, R. Benoit, J. Perron, and C. Masson (2013), Atmospheric icing severity: Quantification and mapping, *Atmos. Res.*, *128*, 57–75, doi:10.1016/j.atmosres.2013.03.005.

Makkonen, L. (2000), Models for the growth of rime, glaze, icicles and wet snow on structures, *Philos. Trans. R. Soc. London*, *358*, 2913–2939, doi:10.1098/rsta.2000.0690.

Makkonen, L., and E. P. Lozowski (2008), Numerical modelling of icing on power network equipment, *Atmos. Icing Power Networks*, *2008*, 83–117.

Marwitz, J. D., M. K. Politovich, B. C. Bernstein, F. M. Ralph, P. J. Neiman, R. Ashenden, and J. Bresch (1997), Meteorological conditions associated with the ATR-72 aircraft accident near Roselawn, Indiana, on 31 October 1994, *Bull. Am. Meteorol. Soc.*, *78*, 41–52, doi:10.1175/1520-0477(1997)078<0041:MCAWTA>2.0.CO;2.

Medina, S., and R. A. Houze (2003), Air motions and precipitation growth in alpine storms, *Q. J. R. Meteorol. Soc.*, *129*, 345–371, doi:10.1256/qj.02.13.

Minder, J. R., D. R. Durran, and G. H. Roe (2011), Mesoscale controls the mountainside snow line, *J. Atmos. Sci.*, *68*, 2107–2127, doi:10.1175/JAS-D-10-05006.1.

Mlawer, E. J., S. J. Taubman, P. D. Brown, M. J. Iacono, and S. A. Clough (1997), Radiative transfer for inhomogeneous atmospheres: RRTM, a validated correlated-k model for the longwave, *J. Geophys. Res.*, *102*, 16,663–16,682, doi:10.1029/97JD00237.

Mott, R., D. Scipión, M. Schneebeli, N. Dawes, A. Berne, and M. Lehning (2014), Orographic effects on snow deposition patterns in mountainous terrain, *J. Geophys. Res. Atmos.*, *119*, 1419–1439, doi:10.1002/2013JD019880.

Musilek, P., D. Arnold, and E. P. Lozowski (2009), An ice accretion forecasting system (IAFS) for power transmission lines using numerical weather prediction, *Sci. Online Lett. Atmos.*, *5*, 25–28, doi:10.2151/sola.2009007.

Niu, S. J., Y. Zhou, R. Jia, J. J. L. Yang, Y. M. Ke, and Z. B. Yang (2012), The microphysics of ice accretion on wires: Observations and simulations, *Sci. China Earth Sci.*, *55*, 428–437, doi:10.1007/s11430-011-4325-8.

Norrman, J., M. Eriksson, and S. Lindqvist (2000), Relationships between road slipperiness, traffic accident risk and winter road maintenance activity, *Clim. Res.*, *15*, 185–193, doi:10.3354/cr015185.

Nygaard, B. E. K., J. E. Kristjnsson, and L. Makkonen (2011), Prediction of in-cloud icing conditions at ground level using the WRF model, *J. Appl. Meteorol. Climatol.*, *50*, 2445–2459, doi:10.1175/JAMC-D-11-054.1.

Pobanz, B. M., J. D. Marwitz, and M. K. Politovich (1994), Conditions associated with large-drops regions, *J. Appl. Meteorol.*, *33*, 1366–1372.

Podolskiy, E. A., B. E. K. Nygaard, L. M. E. Nishimura, and P. Lozowski (2012), Study of unusual atmospheric icing at Mount Zao, Japan, using the weather research and forecasting model, *J. Geophys. Res.*, *117*, D12106, doi:10.1029/2011JD017042.

Pruppacher, H. R., and J. D. Klett (1997), *Microphysics of Clouds and Precipitation*, 945 pp., Kluwer Acad., Dordrecht, Netherlands.

Rasmussen, R., B. C. Bernstein, M. Murakami, G. Stossmeister, J. Reisner, and B. Stankov (1995), The 1990 valentine day arctic outbreak. Part I: Mesoscale and microscale structure and evolution of a Colorado front range shallow upslope cloud, *J. Appl. Meteorol.*, *34*, 1481–1511.

Rauber, R. M., L. S. Olthoff, M. K. Ramamurthy, and K. E. Kunkel (2000), The relative importance of warm rain and melting processes in freezing precipitation events, *J. Appl. Meteorol.*, *39*, 1185–1195, doi:10.1175/1520-0450(2000)039<1185:TRIOWR>2.0.CO;2.

Rauber, R. M., L. S. Olthoff, M. K. Ramamurthy, and D. Miller (2001), A synoptic weather pattern and sounding-based climatology of freezing precipitation in the United States East of the Rocky Mountains, *J. Appl. Meteorol.*, *40*, 1724–1747, doi:10.1175/1520-0450(2001)040<1724:ASWPAS>2.0.CO;2.

Reinking, R. F., and J. F. Boatman (1986), Upslope precipitation events, in *Mesoscale Meteorology and Forecasting*, edited by P. S. Ray, pp. 437–471, Am. Meteorol. Soc., Boston.

Robbins, C. C., and J. V. Cortinas (2002), Local and synoptic environments associated with freezing rain in the contiguous United States, *Weather Forecasting*, *17*, 47–65, doi:10.1175/1520-0434(2002)017<0047:LASEAW>2.0.CO;2.

Roberts, E., and R. E. Stewart (2008), On the occurrence of freezing rain and ice pellets over the eastern Canadian Arctic, *Atmos. Res.*, *89*, 93–109, doi:10.1016/j.atmosres.2007.11.032.

Robichaud, A. J., and G. L. Austin (1988), On the modeling of warm orographic rain by the seeder-feeder mechanism, *Q. J. R. Meteorol. Soc.*, *114*, 967–988, doi:10.1002/qj.49711448207.

Rock, P. A. (2003), *Chemical Thermodynamics*, 548 pp., Univ. Sci. Books.

Roe, G. H. (2005), Orographic precipitation, *Annu. Rev. Earth Planet. Sci.*, *33*, 645–671, doi:10.1146/annurev.earth.33.092203.122541.

Roebber, P. J., and J. R. Gyakum (2003), Orographic influences on the mesoscale structure of the 1998 ice storm, *Mon. Weather Rev.*, *131*, 27–50, doi:10.1175/1520-0493(2003)1312.0.CO;2.

Rosenfeld, D., et al. (2013), The common occurrence of highly supercooled drizzle and rain near the coastal regions of the western United States, *J. Geophys. Res. Atmos.*, *118*, 9819–9833, doi:10.1002/jgrd.50529.

Rowe, A. K., S. A. Rutledge, and T. J. Lang (2012), Investigation of microphysical processes occurring in organized convection during NAME, *Mon. Weather Rev.*, *140*, 2168–2187, doi:10.1175/MWR-D-11-00124.1.

Saleeby, S. M., W. R. Cotton, D. Lowenthal, R. D. Borys, and M. A. Wetzel (2009), Influence of cloud condensation nuclei on orographic snowfall, *J. Appl. Meteorol. Clim.*, *48*, 903–922, doi:10.1175/2008JAMC1989.1.

Sibley, A. (2005), Analysis of the heavy orographic rainfall over North Wales, 2 and 4 February 2004, *Weather*, *60*, 31–36, doi:10.1256/wea.155.04.

Skamarock, W. C., and J. B. Klemp (2008), A time-split nonhydrostatic atmospheric model for weather research and forecasting applications, *J. Comput. Phys.*, *227*, 3465–3485, doi:10.1016/j.jcp.2007.01.037.

Skamarock, W. C., J. B. Klemp, J. Dudhia, D. O. Gill, and D. M. Barker (2008), A description of the advanced research WRF version 3, *NCAR Tech. Note TN-475+STR*, Mesoscale and Microscale Meteorology Division National Center for Atmospheric Research, Boulder, Colo., doi:10.5065/D68S4MVH.

Strapp, J. W., R. A. Stuart, and G. A. Isaac (1996), A Canadian climatology of freezing precipitation, and a detailed study using data from St. John's, Newfoundland, in *Proc. Int. Conf. on Aircraft Inflight Icing*, vol. 2, pp. 45–56, Fed. Aviat. Admin., Springfield, Va.

Stuart, R., and G. Isaac (1999), Freezing precipitation in Canada, *Atmos. Ocean*, *37*, 87–102, doi:10.1080/07055900.1999.9649622.

Sun, J., and S. Zhao (2010), The impacts of multiscale weather systems on freezing rain and snowstorms over southern China, *Weather Forecasting*, *25*, 388–407, doi:10.1175/2009WAF2222253.1.

Tao, W. K., et al. (2009), Goddard multi-scale modeling systems with unified physics, *Ann. Geophys.*, *27*, 3055–3064.

Thompson, G., R. M. Rasmussen, and K. Manning (2004), Explicit forecasts of winter precipitation using an improved bulk microphysics scheme. Part I: Description and sensitivity analysis, *Mon. Weather Rev.*, *132*, 519–542, doi:10.1175/1520-0493(2004)132<0519:EFOWPU>2.0.CO;2.

Thompson, G., P. R. Field, R. M. Rasmussen, and W. D. Hall (2008), Explicit forecasts of winter precipitation using an improved bulk microphysics scheme. Part II: Implementation of a new snow parameterization, *Mon. Weather Rev.*, *136*, 5095–5115, doi:10.1175/2008MWR2387.1.

Thorkildson, R. M., K. F. Jones, and M. K. Emery (2009), In-cloud icing in the Columbia basin, *Mon. Weather Rev.*, *137*, 4369–4381, doi:10.1175/2009MWR2941.1.

Viale, M., R. A. Houze, and K. L. Rasmussen (2013), Upstream orographic enhancement of a narrow cold-frontal rainband approaching the Andes, *Mon. Weather Rev.*, *142*, 1074–1092, doi:10.1175/MWR-D-12-00138.1.

Wang, P. K. (2013), *Physics and Dynamics of Clouds and Precipitation*, 467 pp., Cambridge Univ. Press, New York.

Woods, C. P., M. T. Stoelinga, J. D. Locatelli, and P. V. Hobbs (2005), Microphysical processes and synergistic interaction between frontal and orographic forcing of precipitation during the 13 December 2001 IMPROVE-2 event over the Oregon Cascades, *J. Atmos. Sci.*, *62*, 3493–3519, doi:10.1175/JAS3550.1.

Yang, J., Z. Li, F. L. Yang, and T. Z. Huang (2008), Analysis of the features of covered ice and collapsed tower of transmission line snow and ice attacked in 2008, *Adv. Power Syst. Hydroelectric Eng.*, *24*, 4–8.

Yang, J., K. Jones, W. Yu, and R. Morris (2012), Simulation of in-cloud icing events on Mount Washington with the GEM-LAM, *J. Geophys. Res.*, *117*, D17204, doi:10.1029/2012JD017520.

Zhou, Y., S. J. Niu, and J. J. Lu (2013), The influence of freezing drizzle on wire icing during freezing fog events, *Adv. Atmos. Sci.*, *30*, 1053–1069, doi:10.1007/s00376-012-2030-y.